On the Construction of Invertible Filter Banks on the 2-Sphere

B.T. Thomas Yeo Wanmei Ou Polina Golland

Abstract

The theories of signal sampling, filter banks, wavelets and "overcomplete wavelets" are well-established for the Euclidean spaces and are widely used in the processing and analysis of images. While recent advances have extended some filtering methods to spherical images, many key challenges remain. In this paper, we develop theoretical conditions for the invertibility of filter banks under continuous spherical convolution. Furthermore, we present an analogue of Papoulis's generalized sampling theorem on the 2-Sphere. We use the theoretical results to establish a general framework for the design of invertible filter banks on the sphere and demonstrate with examples of self-invertible spherical wavelets and steerable pyramids.

Index Terms

spheres, frequency response, wavelet transforms, filtering, channel bank filters, image sampling, image orientation analysis, feature extraction

I. Introduction

Multiscale filtering methods, such as wavelets [6] and "overcomplete wavelets" [8], [21], [20] have many applications in feature detection, compression and denoising of planar images. Extending the theories and the methods of filtering to spherical images promises similar benefits in the fields that give rise to such images, including shape analysis in computer vision [4], illumination computation in computer graphics [18], cosmic background radiation analysis in astrophysics [25] and brain cortical surface analysis in medical imaging [28].

This work is funded in part by the NIH NIBIB NAMIC (U54-EB005149), the NIH NCRR mBIRN (U24-RR021382), the NIH NCRR NAC (P41- RR13218), and the NIH NINDS R01-NS051826 grant. B.T. Thomas Yeo is funded by Agency for Science, Technology and Research, Singapore. Wanmei Ou is supported by the NSF graduate fellowship.

We propose a two-stage filtering framework (Figure 1(a)), conceptually equivalent to the usual Euclidean filtering framework except the planar images and filters are replaced by spherical ones. We can think of the first set of filters as analysis filters which project the input image onto the space spanned by the analysis filters. A reconstructed image is then obtained by passing the intermediate outputs through the second layer of filters. Figure 1(b) shows a modification of the framework in Figure 1(a) that introduces sampling between the first and the second layers of filters. The sampling is useful if one is interested in processing the outputs of the analysis filters before passing them through the synthesis filters.

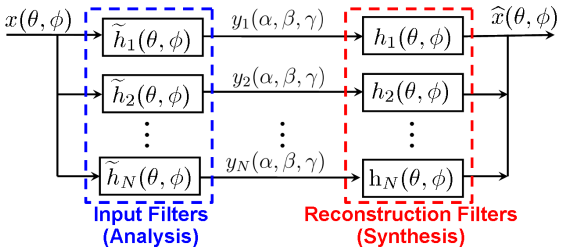

(a) Continuous filter bank

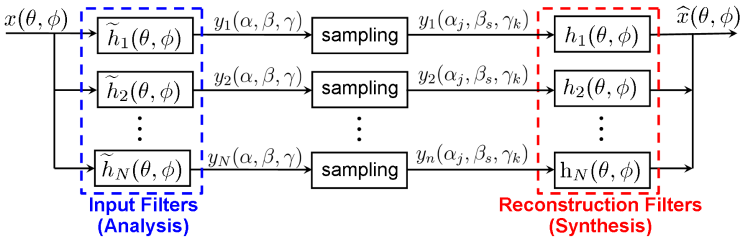

(b) Discrete filter bank

Fig. 1. Continuous and discrete filter bank diagram.

In this work, we analyze the relationship between the reconstructed image and the original image, and establish conditions under which the reconstructed image is the same as the original one, i.e., conditions for invertibility. We demonstrate the use of our results on continuous invertibility and generalized sampling for designing filter banks that enables explicit control of both analysis and synthesis filters. We illustrate the framework by creating examples of self-invertible spherical wavelets and steerable pyramids.

Self-invertibility is desirable for image manipulation in the wavelet domain, because the corresponding analysis and synthesis filters are the same. This leads to an intuitive notion that a convolution coefficient corresponds to the contribution of the corresponding filter to the reconstructed signal. Without self-invertibility, the effects of nonlinear processing of wavelet coefficients could propagate to spatial locations and frequencies other than those which were used to compute the coefficients [20]. To the best of our

knowledge, this is the first approach demonstrated on a sphere that enables design of self-invertible filter banks.

II. Related Work

In the Euclidean domain, the convolution is computed efficiently using the Fast Fourier Transform (FFT) [5]. Once we move to the sphere, FFT must be replaced with an alternative efficient method for computing convolutions. An original algorithm for axis-symmetric convolution kernels on the sphere was derived in [9], and was recently extended to arbitrary functions [24], [26]. These results allow us to efficiently compute the outputs of the first set of filters. Unfortunately, they do not apply to the convolution with the second layer of filters because the outputs of the first layer of filters are in general not spherical images as we will see in section III.

In the past decade, there has been much work on extending the general paradigm of linear filtering to the spherical domain [1], [3], [7], [10], [11], [14], [18], [19], [22], [25]. For example, the lifting scheme in [18], [19] adopts a non-parametric approach to computing wavelet decomposition of arbitrary meshes by generalizing the standard 2-scale relation of Euclidean wavelets. This method enables a multi-scale representation of the original mesh (image) with excellent compression and speed performance. However, the lifting wavelets are not overcomplete, i.e., exactly one wavelet coefficient is created per sample point, causing difficulties in designing filters for oriented feature detection.

A similar problem in the Euclidean domain leads to the invention of “overcomplete wavelets”, such as steerable pyramids [12], [20]. A group theoretic formulation of overcomplete continuous spherical wavelets is proposed in [1]. In particular, it can be shown that the stereographic projection of an admissible planar wavelet to the sphere is also admissible under the group theoretic framework, providing a straightforward framework for the design of analysis filters for specific features of interest, such as oriented edges [25].

In the group theoretic approach, defining the mother wavelet completely determines the analysis and synthesis filters. However, while the analysis filters are related by stereographic dilation, the synthesis filters are in general not related by dilation. In fact, the support of corresponding analysis and synthesis filters is guaranteed to be the same in frequency domain but not in the spatial domain.

Bogdanova *et al.* [3] discretize the group theoretic wavelets, providing a sampling guarantee for the framework of Figure 1(b) for the restricted class of axis-symmetric filters[1]. This work is therefore the

[1]An axis-symmetric spherical function is one which is symmetrical about the north pole.

most similar to ours. In contrast, we study general filter banks, without any restriction on the relationships among the cascade of filters. We derive the analogue of the Papoulis's generalized sampling theorem [15] on the sphere, applicable to both axis-symmetric and axis-asymmetric (or oriented) filters.

Driscoll and Healy [9] provide the equivalent of the Nyquist-Shannon sampling theorem on the sphere. While the Nyquist-Shannon sampling theorem provides reconstruction guarantees for bandlimited signals in Euclidean space under perfect sampling (convolution with a delta function), Papoulis's generalized sampling theorem provides guarantees for bandlimited signals sampled via convolutions with kernels of sufficient bandwidth.

An earlier version of this work was first presented at the International Conference on Image Processing [27]. In this current paper, we include proofs of the invertibility conditions as well as demonstrate the generation of self-invertible spherical steerable pyramids. In the next section, we introduce the notation used throughout the paper. In section IV, we present the main theoretical contributions of this paper: continuous invertibility and the generalized sampling theorem. We propose a procedure for generating self-invertible multiscale filter banks on the sphere in section V. We then illustrate the procedure for the case of wavelets and steerable pyramids in section VI and conclude with the discussion of future research and outstanding challenges in the proposed framework.

III. DEFINITIONS

Let $x(\theta, \phi) \in L^2(S^2)$ be a square-integrable function on the two-dimensional unit sphere, where (θ, ϕ) are the spherical coordinates. Suppose $P = (\theta, \phi)$ is a point on the sphere. Then, $\theta \in [0, \pi]$ is the co-latitude, which is the angle between the positive z-axis (north pole) and the vector corresponding to P. $\phi \in [0, 2\pi]$ is the longitude and is taken to be the angle between the positive x-axis and the projection of P onto the x-y plane. ϕ is undefined on the north and south poles.

The spherical harmonics $Y_l^m(\theta, \phi)$ [17] form an orthonormal set of basis functions for $L^2(S^2)$: i.e.,

$$x(\theta, \phi) = \sum_{l=0}^{\infty} \sum_{|m| \leq l} x^{l,m} Y_l^m(\theta, \phi) \tag{1}$$

where $x^{l,m}$ is the spherical harmonic coefficient of degree l and order m obtained by projecting the function $x(\theta, \phi)$ onto $Y_l^m(\theta, \phi)$:

$$x^{l,m} = \int_{S^2} x(\theta, \phi) Y_l^{m*}(\theta, \phi) d\Omega \tag{2}$$

where $d\Omega = \sin\theta d\theta d\phi$ and * denotes complex conjugation. We call $Y_l^m(\theta, \phi)$ a spherical harmonic of degree l and order m. We note that for axis-symmetric functions (independent of ϕ), only the order 0 harmonics are non-zero. A more detailed background of spherical harmonics is found in Appendix A.

We choose to parameterize rotations on the sphere by the Euler angles, α, β, γ ($\alpha \in [0, 2\pi]$, $\beta \in [0, \pi]$, $\gamma \in [0, 2\pi]$). The rotation operator $D(\alpha, \beta, \gamma)$ first rotates a function by γ about the z-axis (Figure 2(b)), then by β about the y-axis (Figure 2(c)) and finally by α about the z-axis (Figure 2(d)). The direction of positive rotation follows the right-hand screw rule. The three angles specify an element of the rotation group $SO(3)$ and provide a natural parametrization of convolution on the sphere. The effects of rotation on the spherical harmonic coefficients of a function is expressible in terms of the so called Wigner-D functions. The Wigner-D functions form an irreducible representation of the rotation group [17]. Appendix A provides the explicit expressions for the Wigner-D functions.

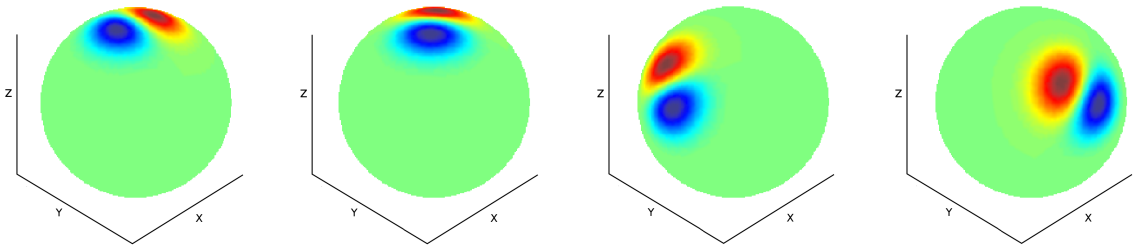

(a) Original spherical image (b) Rotate by γ about z-axis (c) Rotate by β about y-axis (d) Rotate by α about z-axis

Fig. 2. Rotation via euler angles (α, β, γ)

A. Continuous Convolution

On the plane, convolution is defined in terms of the inner product between two functions translated relative to each other, and is parameterized by the amount of translation. On the sphere, it is more natural to talk about rotation rather than translation, and therefore spherical convolution is parameterized by rotation. Given a spherical image $x(\theta, \phi)$ and a spherical filter $\tilde{h}(\theta, \phi)$, their spherical convolution

$$y(\alpha, \beta, \gamma) = \int_{S^2} [D(\alpha, \beta, \gamma)\tilde{h}]^*(\theta, \phi) x(\theta, \phi) d\Omega \tag{3}$$

is a function of $L^2(SO(3))$ rather than $L^2(S^2)$. By convention, we shall consider the center (origin) of a spherical filter to be at the north pole ($\theta = 0$). Then intuitively, $y(\alpha, \beta, \gamma)$ is the inner product between the re-oriented filter $D(\alpha, \beta, \gamma)\tilde{h}$ (e.g., Figure 2(d)) and the spherical image. In other words, we obtain $y(\alpha, \beta, \gamma)$ by first re-orienting the spherical filter by a rotation of γ about the z-axis (center still at north pole) and then bringing the center of the filter to the point (β, α) of the spherical image, and then performing an inner product between the image and filter. Therefore $y(\alpha, \beta, \gamma)$ is the correlation of the rotated version of $\tilde{h}$ with x, or the projection coefficient of x onto $[D(\alpha, \beta, \gamma)\tilde{h}]$. In the case of

the filter shown in Figure 2, a high value of $y(\alpha, \beta, \gamma)$ would imply the presence of an oriented edge at spherical coordinate (β, α) with orientation "γ".

We note that the notion of orientation is inherently local here because a continuous unit-norm vector field does not exist on the sphere. Therefore, it is not meaningful to claim an existence of an edge of orientation γ at location (β, α) without specifying a local coordinate system. In our case, we can define such a local coordinate system by first specifying one at the north pole. Our choice of parameterizing rotation via the Euler angles then induces a local coordinate system everywhere, except the south pole.

For axis-symmetric filters, $\tilde{h}(\theta, \phi) = \tilde{h}(\theta)$, the rotation by γ about z-axis has no effect, i.e., $y(\alpha, \beta, \gamma) = y(\alpha, \beta)$ is a spherical image parametrized by $\theta = \beta, \phi = \alpha$. Our definition of convolution is identical to that in [24], [26], although [26] calls it directional correlation. In [9], γ is integrated out, resulting in a spherical image.

The convolution of a spherical filter $h(\theta, \phi)$ with $y(\alpha, \beta, \gamma) \in L^2(SO(3))$ produces a spherical image:

$$\widehat{x}_h(\theta, \phi) = \int_{SO(3)} [D(\alpha, \beta, \gamma)h](\theta, \phi) y(\alpha, \beta, \gamma) d\rho \tag{4}$$

where the integration is over the Euler angles: $d\rho = \sin\beta d\alpha \, d\beta \, d\gamma$. We can think of the inverse convolution in the following way. The reconstructed value at a given (θ, ϕ) is obtained by summing (integrating) the contributions of the rotated reconstruction filters h, centered at (β, α) and oriented by γ (e.g., Figure 2(d)), where the weights of the contributions are given by the convolution outputs (projection coefficients on the corresponding input filters).

When using a filter bank of N analysis-synthesis filter pairs (Figure 1(a)), the reconstructed signal is obtained by summing the response of all filter pairs:

$$\widehat{x}(\theta, \phi) = \sum_{n=1}^{N} \int_{SO(3)} [D(\alpha, \beta, \gamma)h_n](\theta, \phi) y_n(\alpha, \beta, \gamma) d\rho \tag{5}$$

which is analogous to the definition in [1], with integration over scale replaced by summation over the filter index.

B. Discrete Convolution

In the Euclidean case, we typically discretize both the input images and the convolution outputs. When working on the sphere, we choose to keep the image domain continuous by working with spherical harmonic coefficients rather than sample values, because this allows us to exploit efficient algorithms for spherical convolution [24], [26]. Since no uniform sampling grid exists on the sphere, performing convolution completely by quadrature would be slow. This is because under each rotation of the filter relative to the spherical image, we will need to re-sample (or re-interpolate) the filter or the image.

For $L^2(SO(3))$ (or equivalently, in the spherical wavelet domain), continuous representation is possible through series of complex exponentials [24] or Wigner-D functions [26]. However, both the complex exponentials and the Wigner-D functions have global support. Therefore in applications where we want to modify the image in the wavelet domain, manipulating the series coefficients would be tantamount to simultaneously altering all the wavelet coefficients, defeating the purpose of the wavelet decomposition, which is to provide localized control in both spatial and frequency domain. To avoid this, we sample the output of the continuous convolution $y(\alpha, \beta, \gamma)$ to create its discrete counterpart $y(\alpha_j, \beta_s, \gamma_k)$, where $\{\alpha_j, \beta_s, \gamma_k\}$ define a particular sampling grid (Figure 1(b)). The convolution between the sampled projection coefficients $y_{j,s,k}$ and the continuous reconstruction filters h is then defined as:

$$\widehat{x}_h(\theta, \phi) = \sum_{j=0}^{J-1} \sum_{s=0}^{S-1} \sum_{k=0}^{K-1} w_{j,s,k} [D(\alpha_j, \beta_s, \gamma_k)h](\theta, \phi) y(\alpha_j, \beta_s, \gamma_k) \tag{6}$$

which includes sampling-dependent quadrature weights $w_{j,s,k}$, introduced so that the discrete case converges to the continuous case as the number of samples increases. This definition allows for an easy transfer of continuous filtering theory to its discrete analogue. In the next section, we show that "good" choices of $w_{j,s,k}$ exist depending on the sampling schemes. In contrast with the Euclidean case, $w_{j,s,k}$ are necessary because of the non-uniform measure on the Euler angles $d\rho = \sin\beta d\alpha d\beta d\gamma$, as we discuss in section IV.

Similar to the continuous case (cf. Eq. (4)), the signal reconstructed through N analysis-synthesis filter pairs is defined as a sum of contributions of all filter pairs:

$$\widehat{x}(\theta, \phi) = \sum_{n=1}^{N} \sum_{j=0}^{J_n-1} \sum_{s=0}^{S_n-1} \sum_{k=0}^{K_n-1} w_{j,s,k,n} [D(\alpha_{j,n}, \beta_{s,n}, \gamma_{k,n})h_n](\theta, \phi) y_n(\alpha_{j,n}, \beta_{s,n}, \gamma_{k,n}) \tag{7}$$

The sampling grid and the quadrature weights now depend on n since different filters in the filter bank might use different sampling schemes.

IV. Invertibility Conditions

In this section, we present the main theoretical contributions of our work.

Theorem 4.1: **(Continuous Frequency Response)**. Let $\{\widetilde{h}_n, h_n\}_{n=1}^N$ be an analysis-synthesis filter bank. Then for any spherical image $x \in L^2(S^2)$ and its corresponding reconstructed image $\widehat{x}$,

$$\hat{x}^{l,m} = x^{l,m} \frac{8\pi^2}{2l+1} \left\{ \sum_{n=1}^{N} \sum_{m'=-l}^{l} \left[h_n^{l,m'} \right] \left[\widetilde{h}_n^{l,m'} \right]^* \right\} \tag{8}$$

where $x^{l,m}$ and $\widehat{x}^{l,m}$ are the spherical harmonic coefficients of the input and reconstructed signals respectively, $\widetilde{h}_n^{l,m'}$ and $h_n^{l,m'}$ are the spherical harmonic coefficients of the n-th analysis and synthesis filters respectively.

Appendix B presents the proof of Theorem 4.1. To draw an analogy with the Euclidean case, we call

$$H_{\widetilde{h},h}(l) \;=\; \frac{8\pi^2}{2l+1}\sum_{n=1}^{N}\sum_{m'=-l}^{l}\left[h_n^{l,m'}\right]\left[\widetilde{h}_n^{l,m'}\right]^* \tag{9}$$

the frequency response of the analysis-synthesis filter bank. Note that the degree l spherical harmonics coefficients of the reconstructed signal are affected only by the degree l spherical harmonic coefficients of the filters. However, the degree l order m spherical harmonic coefficient of the reconstructed signal is affected by all the orders of degree l spherical harmonic coefficients of the filters. In contrast, on the plane, the frequency response is simply the sum of products of the Fourier coefficients of the analysis and the synthesis filters:

$$\mathcal{F}\{\widehat{x}\}(s_1,s_2) \;=\; \mathcal{F}\{x\}(s_1,s_2)\sum_{n=1}^{N}\mathcal{F}\{h_n\}(s_1,s_2)\mathcal{F}\{\widetilde{h}_n\}(s_1,s_2) \tag{10}$$

where $\mathcal{F}\{\widehat{x}\}(s_1,s_2)$, $\mathcal{F}\{x\}(s_1,s_2)$, $\mathcal{F}\{\widetilde{h}_n\}(s_1,s_2)$ and $\mathcal{F}\{h_n\}(s_1,s_2)$ denote the fourier transforms of the reconstructed signal, original signal, analysis filters and synthesis filters respectively. We see that the effects of s_1 and s_2 are separable, unlike l and m. Furthermore, on the sphere, the frequency response contains an extra modulating factor that decreases with degree l. The following corollary of Theorem 4.1 provides the necessary and sufficient condition for the invertibility of filter banks under continuous convolution.

Corollary 4.2: **(Continuous Invertibility)**. Let $\{\widetilde{h}_n, h_n\}_{n=1}^{N}$ be an analysis-synthesis filter bank. Then for any spherical image $x \in L^2(S^2)$ and its corresponding reconstructed image $\widehat{x}$,

$$\hat{x}^{l,m} = x^{l,m} \;\text{ for all }\; (l,m) \quad \text{iff} \quad \sum_{n=1}^{N}\sum_{m'=-l}^{l}\left[h_n^{l,m'}\right]\left[\widetilde{h}_n^{l,m'}\right]^* = \frac{2l+1}{8\pi^2} \;\text{ for all }\; l\; s.t.\; x^{l,m}\neq 0 \tag{11}$$

We note that the corollary is easily satisfied if there are no constraints on the relationships among the cascade of filters: given a set of analysis filters $\widetilde{h}_n$, there are in general multiple sets of synthesis filters that can achieve invertibility. For example, we can define the synthesis filters to be $h_n = L_\psi \widetilde{h}_n$, where,

$$[L_\psi \widetilde{h}_n]^{l,m} \;=\; \begin{cases} \frac{1}{H_{\widetilde{h},\widetilde{h}}(l)}\widetilde{h}_n^{l,m} & \text{for } H_{\widetilde{h},\widetilde{h}}(l) > 0 \\ 0 & \text{otherwise} \end{cases} \tag{12}$$

and $H_{\widetilde{h},\widetilde{h}}(l)$ is the frequency response defined in Eq. (9). L_ψ is a frequency modulating operator that normalizes the synthesis filters at each degree, such that the combined frequency response of the filter bank is 1 for all l with $H_{\widetilde{h},\widetilde{h}}(l) > 0$. This filter bank is therefore invertible over the frequency range of the support of the filters. This operation is similar to the frame operator in the continuous spherical wavelet transform of [1], where the counterpart of $H_{\widetilde{h},\widetilde{h}}(l)$ is given by $\frac{8\pi^2}{2l+1}\sum_{|m|\leq l}\int_0^\infty \frac{1}{a^3}|\widetilde{h}_a^{l,m}|^2 da$, replacing the summation over n by the integration over the scale a, with measure $\frac{1}{a^3}da$. For the special case of

the analysis filters being dilated versions of each other, this choice of the synthesis filters is a direct discretization of [1], albeit ignoring the measure of a. The complete discretization of the continuous wavelet transform in [1] is actually accomplished in [3]. However, regardless of using L_ψ or the frame operators of [1], [3], the synthesis filters are in general not related by dilation even if the analysis filters are.

We now define $L_{\widetilde{h}_n}(O_{\widetilde{h}_n})$ and $L_{h_n}(O_{h_n})$ to be the highest non-zero harmonic degree (order) of $\widetilde{h}_n$ and h_n respectively. The following result specifies the sufficient, but not necessary, conditions for the invertibility of filter banks under the sampling framework of Figure 1(b).

Theorem 4.3: **(Generalized Sampling Theorem)**. Let $\{\widetilde{h}_n,\, h_n\}_{n=1}^N$ be a filter bank whose frequency response defined by Eq. (9) is equal to 1 up to degree $L < \infty$ and $O_{\widetilde{h}_n} < \infty$ and $O_{h_n} < \infty$. Let $\widetilde{L}_n = \min(L, L_{\widetilde{h}_n})$ and the sampling grid and the quadrature weights satisfy

- $\alpha_{j,n} = \frac{2\pi j}{\widetilde{L}_n + L + 1}$ for $j = 0, 1, \ldots, (\widetilde{L}_n + L)$
- $\gamma_{k,n} = \frac{2\pi k}{O_{\widetilde{h}_n} + O_{h_n} + 1}$ for $k = 0, 1, \ldots, (O_{\widetilde{h}_n} + O_{h_n})$
- $w_{s,n}$ and $\beta_{s,n}$ are the quadrature weights and knots such that

$$\int_0^\pi d^l_{mm'}(\beta) d^{l'}_{mm'}(\beta) \sin(\beta) d\beta = \sum_{s=0}^{S_n - 1} w_{s,n} d^l_{mm'}(\beta_{s,n}) d^{l'}_{mm'}(\beta_{s,n}) \tag{13}$$

  for $l \leq L, l' \leq \widetilde{L}_n$, where $d^l_{mm'}(\beta)$ and $d^{l'}_{mm'}(\beta)$ are the Wigner-d functions.

- $w_{j,s,k,n} = \frac{4\pi^2 w_{s,n}}{(\widetilde{L}_n + L + 1)(O_{\widetilde{h}_n} + O_{h_n} + 1)}$

Then the filter bank is invertible for any spherical image $x \in L^2(S^2)$ with maximum degree L (i.e., $\widehat{x}^{l,m} = x^{l,m}$ for all $0 \leq l \leq L$) under the discrete convolution of Figure 1(b).

Appendix A provides the definitions and the explicit expressions for the Wigner-d functions. We emphasize the need for the input signal x to be bandlimited. Furthermore, the spherical harmonic coefficients of $\widehat{x}$ might not be zero for degrees beyond L. The constraints in this theorem ensure that the number of samples remain finite. The samples and the weights are picked such that the discrete reconstruction obtained in Eq. (7) is the same as the continuous result in Eq. (5) up to degree L. The proof is found in Appendix C. In Appendix D, we demonstrate two sets of quadrature weights and knots that satisfy the conditions of the theorem.

The theorem is sufficient rather than necessary because other quadrature schemes that enable perfect reconstruction can exist. Subtle variations of the theorem can also be obtained, for example by increasing the maximum degree of the input signal x to be greater than L or increasing the number of samples on α and β or both.

The measures corresponding to α and γ are constants in $SO(3)$, just like in the Euclidean space. We therefore assume uniform sampling for these parameters in our work. For discrete planar convolution, it is customary to have no weights (or rather, unit weights). On the sphere, however, the non-uniform measure on β, $\sin\beta d\beta$, presents challenges for sampling. If we are simply interested in convergence, then setting $w_{j,s,k} = \frac{2\pi}{J}\frac{2\pi}{S}\sin(\beta_s)\frac{2\pi}{K}$ for uniform samples of α, β, γ corresponds to the Riemann sum of the integral. Theorem 4.3 states that better quadrature schemes exist that guarantee exact reconstruction up to a certain bandwidth.

The generalized sampling theorem is useful for the perfect reconstruction of an original signal sampled with equipment that introduced blurring during the acquisition process. For example, the first layer of filters $\widetilde{h}_n$ could be the blurring kernels of a set of N radio dishes measuring the cosmic background radiation of the sky. We can then hope to recover the true cosmic background radiation signal by passing the recorded signal through the second bank of filters.

The two theorems imply that if a filter bank with a finite maximal spherical harmonic order is invertible up to degree L under the continuous spherical convolution, it is also invertible up to degree L under the discrete spherical convolution. Because functions in $L^2(S^2)$ have finite energy, their spherical harmonic coefficients must necessarily decay to zero. Therefore we can reasonably assume that the filters of the filter bank are of finite bandwidth as required by Theorem 4.3 and that we can represent the filters with a finite number of coefficients up to an arbitrary pre-specified precision. We will therefore focus on constructing invertible filter banks for continuous convolution.

V. Constructing Self-Invertible Multiscale Filter Banks

In this section, we outline the use of the continuous invertibility corollary to generate self-invertible multiscale filter banks. The optimization framework presented here can be easily adapted to design other types of filter banks by altering the structure of the optimization problem according to an application's needs.

For self-invertible filter banks, $\widetilde{h}_n(\theta,\phi)$ is constrained to be the same as $h_n(\theta,\phi)$. Furthermore, in multi-scale analysis, the analysis filters are related through dilation and scaling of a particular template $\widetilde{h}(\theta,\phi)$, i.e.,

$$\widetilde{h}_n(\theta,\phi) = (\prod_{k=1}^{n} b_k) D_{a_n} \widetilde{h}(\theta,\phi) \tag{14}$$

where $b_k \geq 1$ and D_{a_n} is the nonlinear dilation operator[2], with larger n corresponding to smaller a (narrower filters).

In this paper, we adopt the stereographic dilation operator introduced in [1], which involves stereographically projecting the function from the sphere onto the plane, performing the usual dilation operation on the plane and then projecting the resulting function back onto the sphere[3]. Stereographic dilation allows for an explicit control of the spatial localization of the wavelets in contrast with previous approaches that define dilation in the frequency domain [3].

The definition of the stereographic dilation includes a normalization factor such that the inner product between functions is conserved:

$$[D_a f](\theta,\phi) = \frac{1}{a}\left(\frac{1+\tan^2\frac{\theta}{2}}{1+(\frac{1}{a}\tan\frac{\theta}{2})^2}\right) f(2\tan^{-1}(\frac{1}{a}\tan\frac{\theta}{2}),\phi) \tag{15}$$

Because of the nonlinear nature of stereographic dilation, extreme dilation of a spherical function will eventually lead to high frequencies. In practice, we will avoid working in that region, since the dilated filter no longer looks like the original filter.

The b_k's in Eq. (14) are the amplitude scaling parameters that control the tradeoff between self-invertibility and norm-preserving dilation. Corollary 4.2 implies that the sum of squares of the spherical harmonic coefficients of a bank of self-invertible filters must increase linearly with degree. But stretching a function while preserving its norm shifts its spherical harmonic coefficients to the left (spherical harmonic degrees decrease) and magnifies them (Figure 3).

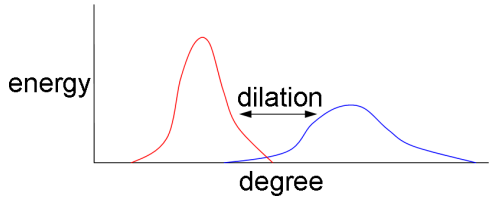

Fig. 3. Effect on energy due to norm preserving stereographic dilation.

[2]We note that the symbol D is overloaded to imply rotation as well as dilation, but the meaning should be clear depending on the context.

[3]We note that the approach commonly used with planar images of applying a constant filter to a subsampled image fails here because the sphere is periodic and bounded, causing the effective size of the features (relative to the filter) to stay constant with subsampling. We also note that nonlinear dilation is necessary since the sphere is compact, hence dilating a spherical function by naively scaling the radial component of the spherical function, $f(\theta,\phi) \rightarrow f(\frac{\theta}{a},\phi)$, leads to undesired "wrap-around" effects.

These extra weights are analogous to the measure of scale $\frac{1}{a^3}da$ in the group theoretic formulation of wavelets [1], which results in wider filters being assigned smaller weights. On the continuous real line, the measure $\frac{1}{a^2}da$ nicely cancels out the dilation of the filter (cf. [23], chapter 5). On the discrete real line, the convolution outputs of narrower filters are sampled more densely. This suggests two possible approaches: variable sampling of the convolution outputs or variable scaling of the filters. Because the effects of stereographic dilation on the spherical harmonic coefficients of a function is not analytical, neither approach leads to a closed-form solution. In this paper, we take the variable scaling approach by finding the appropriate b_k's as part of the filter design.

Fortunately, stereographic dilation is distributive over addition. Suppose the template $\widetilde{h}$ is expressible as a linear combination of the basis functions $B^i(\theta,\phi)$, i.e., $\widetilde{h}(\theta,\phi) = \sum_{i=1}^{M} c_i B^i(\theta,\phi)$. Here, we assume that $B^i(\theta,\phi)$ are spherical harmonics and note that the technique is still applicable if a more suitable basis is found. Applying stereographic dilation to $\widetilde{h}$,

$$[D_a\widetilde{h}]^{l,m} = \left[D_a \sum_{i=1}^{M} c_i B^i\right]^{l,m} = \sum_{i=1}^{M} c_i [D_a B^i]^{l,m} \tag{16}$$

yields the spherical harmonic coefficients of the analysis filter at another scale. This is useful since the invertibility condition in Corollary 4.2 is expressed in terms of the spherical harmonic coefficients of the filters. We can therefore decide on a set of scales $\{a_n\}_{n=1}^{N}$ and create a table of spherical harmonic coefficients of the dilated basis functions. Eq. (16) allows us to determine the spherical harmonic coefficients of the dilated filters at each relative scale given c_i's and b_k's. This technique can also be applied to other definitions of scale that are distributive over addition.

After fixing the set of basis functions $\{B^i\}$ and the set of scales $\{a_n\}$, we now pose an optimization problem to determine c_i's and b_k's. Similarly to the filter design in the Euclidean space, the objective function should be application dependent, and could for example be a function of the frequency response. The constraints come from enforcing self-invertibility: we assume that the analysis and synthesis filters are identical and optimize the cost function under the invertibility constraints of Corollary 4.2. Since we cannot have more constraints than variables, self-invertibility cannot be achieved for more degrees than the number of basis functions and scales. We will discuss examples of the objective function in section VI.

The quadratic penalty method [2] is effective in solving this optimization problem with non-convex constraints by incorporating the constraints into the objective function and solving the resulting uncon-

strained optimization problem using non-linear least squares optimization [4]. The procedure is repeated while increasing the weights of the constraints and using the solution corresponding to the previous weights as the starting point, until convergence to a local minimum of the original cost function.

VI. EXPERIMENTS

In this section, we demonstrate the optimization procedure formulated in the previous section. We demonstrate the construction of both self-invertible spherical wavelets and spherical steerable pyramids. Similar to the Euclidean domain, we define a spherical wavelet transform to be the decomposition of a spherical signal into component signals at different scales, i.e., employing axis-symmetric filter kernels. On the other hand, we reserve the term spherical steerable pyramid transform for the decomposition of a spherical signal into component signals at different scales and orientations, i.e., using axis-asymmetric filter kernels. We note that in some literature [1], [3], [25], the term "spherical wavelets" includes spherical steerable pyramids.

A. Spherical Wavelets

In designing axis-symmetric wavelets, we limit our set of basis functions $\{B^i\}$ to be the first hundred spherical harmonics of order 0, since the spherical harmonic coefficients of axis-symmetric functions are zero for orders other than 0.

We define the set of scales to be $a = \{2^{-\frac{n}{3}}\}, n = -6, -5, \cdots, 2, 3$, with $a = 1$ corresponding to the undilated template. We use S2kit [13] to create a table of the spherical harmonic coefficients of $D_a Y_l^0$ for $l = 0, \cdots, 99$. We find the first 600 order 0 spherical harmonic coefficients of each dilated spherical harmonic (a dilated axis-symmetric function remains axis-symmetric). As mentioned before, extreme stereographic dilation and shrinking of spherical harmonics can result in high frequencies. We verify that for $a = 4$ and $a = 0.5$, $[D_a Y_{99}^0]^{599,0} < 10^{-7}$.

For axis-symmetric filters, we can use the fast spherical convolution [9] to compute forward convolution. We quote the results here for completeness:

$$[y(\beta, \alpha)]^{l,m} = \sqrt{\frac{4\pi}{(2l+1)}} x^{l,m} \widetilde{h}^{l,0*} \tag{17}$$

An extra multiplier of 2π is introduced in [9] by integrating out γ. We will show in Appendix E that we can use almost the same formula to calculate the convolution of $y(\beta, \alpha)$ with an axis-symmetric filter $h(\theta, \phi)$ in the reconstruction process.

[4]Our implementation uses Matlab's lsqnonlin.

Because we seek to decompose a spherical signal into component signals at different scales, we would like the filter at each scale to act as a bandpass filter. Similar to the Euclidean domain, we require a residual lowpass filter to ensure that the combined wavelet and the lowpass filter bank is invertible up to a particular degree. Since we only use the first 100 spherical harmonics as our basis, the frequency response of $\widetilde{h}_{a=1}(\theta,\phi)$ will be zero for all degrees higher than 99. If we also penalize the magnitude of the leading spherical harmonic coefficients of $\widetilde{h}_{a=1}(\theta,\phi)$, the frequency response of $\widetilde{h}_{a=1}(\theta,\phi)$ will be zeros at both ends, i.e., it will serve as a bandpass filter. To satisfy the self-invertibility conditions, the solution cannot be identically zero, but must rise to a peak somewhere in the middle of the frequency range.

We also penalize the second derivatives of the filters' frequency responses and spherical harmonic coefficients to force the filters to be relatively smooth and to reduce ringing. We can induce a sharper cutoff frequency by penalizing the magnitude of the combined frequency response above a cutoff degree L_c. In addition, we fix the amplitude scaling factors b_k's to be the same. While allowing the b_k's to take on different values provides the optimization procedure more flexibility in finding a set of desired filters, we find that in practice, having the same b for all the scales results in the frequency responses of the filters at all scales having comparable amplitude. Once again, we note that the energies of the filters at different scales will be different because of Corollary 4.2.

Figure 4(a) illustrates the frequency response of a 10-scale wavelet filter bank ($a = \{2^{-\frac{n}{3}}\}$, $n = -6,-5,\cdots,2,3$) obtained through our optimization procedure. Invertibility is enforced from degree 15 to 79. Furthermore, we impose a quadratic penalty on the magnitude of the combined frequency response for degrees above $L_c = 150$. The combined frequency response of the filters is shown in Figure 4(c).

Because the filters are axis-symmetric, we can plot the filters in the image domain as a function of θ (Figure 4(b)). The existence of a second peak after the peak at $\theta = 0$ (north pole) indicates ringing. When we vary the cutoff frequency penalty, we can trade off the amount of ringing for the slope of the cutoff. For example, Figure 5(a) shows the combined frequency response of a wavelet filter bank obtained by penalizing the magnitude of the combined frequency response for degrees above $L_c = 100$. Notice the combined frequency response drops rapidly after degree 79. However, this results in increased ringing. If we measure ringing by the ratio of the second maxima to the maxima at the north pole, we can measure the tradeoff between ringing and the cutoff frequency, as shown in Figure 5(b). As a verification step, we convolve the wavelet filter bank of Figure 4(a) with the world elevation map (Figure 6(a)). The results for 4 scales are shown in Figure 6(b-e). Upon reconstruction using Eq. (92), we find that $|\widehat{x}^{l,m} - x^{l,m}| < 10^{-7}$ for degrees between 15 to 79 inclusive. As mentioned before, a residual lowpass filter is required to ensure

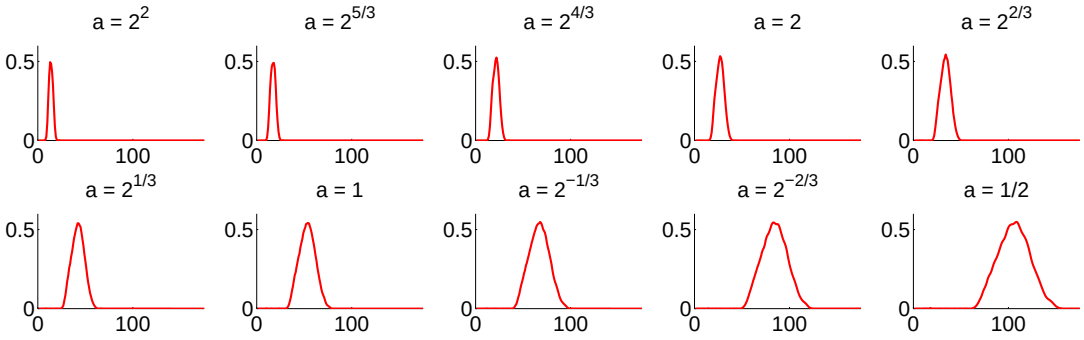

(a) Frequency response of individual filters.

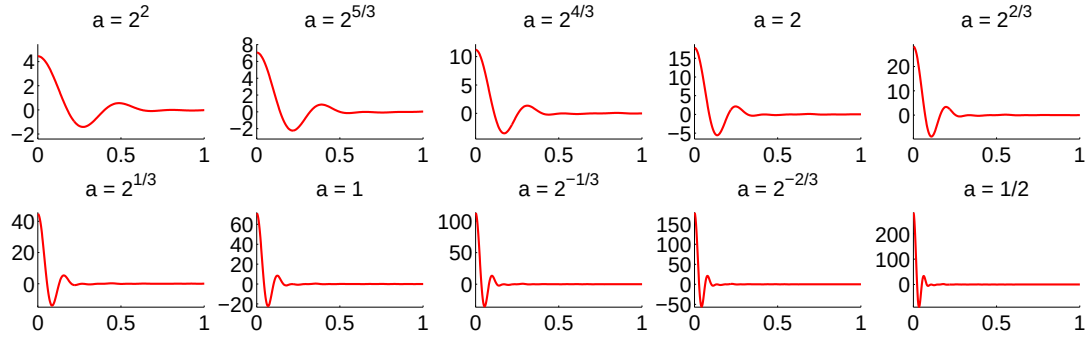

(b) Individual filters in the spatial domain ($0 \leq \theta \leq 1$ radian). The second peak indicates ringing.

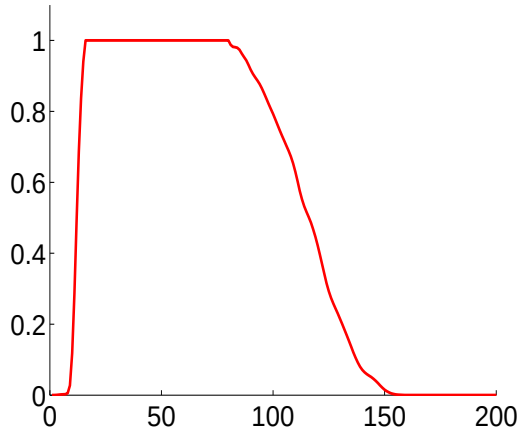

(c) Combined frequency response, $L_c = 150$.

Fig. 4. 10-scale wavelet filter bank obtained by imposing invertibility from degree 15 to 79 and a combined frequency response cutoff at $L_c = 150$.

invertibility up to degree 79.

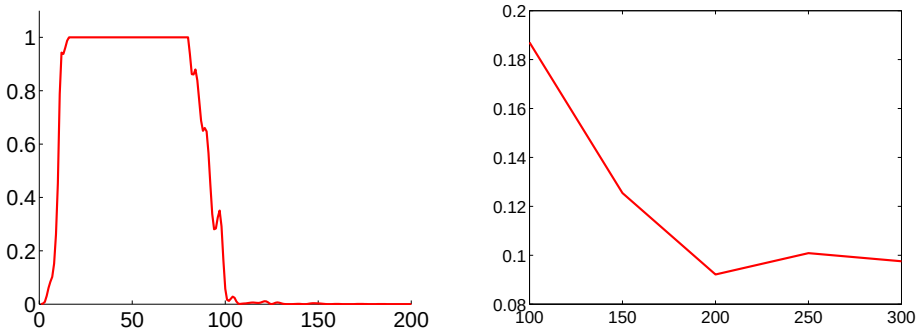

(a) Combined frequency response, $L_c = 100$ (b) Ringing vs L_c

Fig. 5. (a) Combined frequency response of the filters obtained when the combined frequency response cutoff is set to $L_c = 100$. Note the sharper cutoff obtained. However, this is at the expense of ringing. (b) Plot of ringing versus cutoff frequency L_c. Ringing is defined to be the ratio of the second peak to the maximum peak at the lowest scale, $a = 4$.

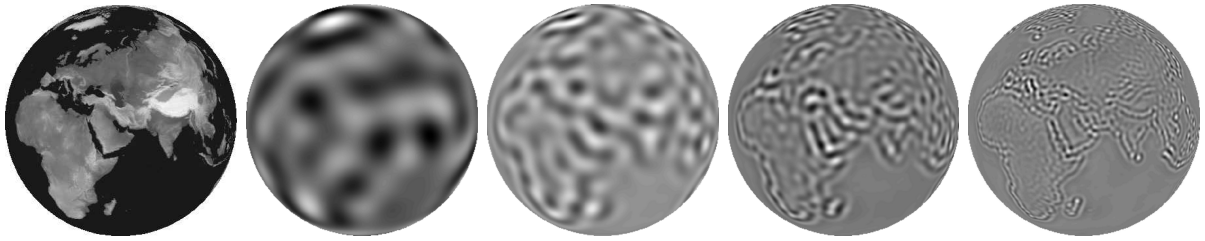

(a) Original Image (b) a = 4 (c) a = 2 (d) a = 1 (e) a = 0.5

Fig. 6. Outputs of the analysis filter bank of Figure 4 applied to the world elevation map. Only 4 scales are shown.

To demonstrate that the optimization procedure is stable across different settings of parameters, we show a second example where we optimize for a 4-scale wavelet filter bank ($a = \{4, 2, 1, 0.5\}$). We enforce invertibility from degree 10 to 89 and apply a quadratic penalty on the magnitude of the combined frequency response for degrees above $L_c = 150$. The combined frequency response of the resultant filter bank is shown in Figure 7(a). Once again, by varying the cutoff frequency threshold, we can obtain a tradeoff between ringing and sharpness of the cutoff (see Figure 7(b)). We apply the filter bank to the world elevation map (see Figure 8) and find that invertibility is obtained for degrees between 10 and 89 inclusive. Notice that there is significantly less ringing artifacts than in Figure 6 as predicted by our measure of ringing at $L_c = 150$ (compare Figure 5(b) and Figure 7(b)).

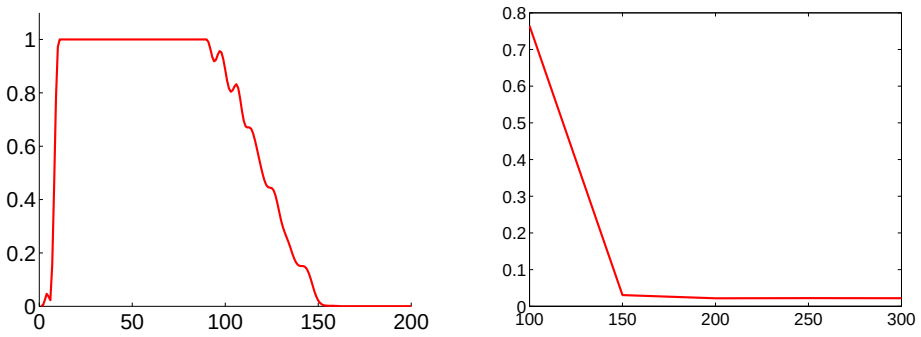

(a) Combined frequency response, $L_c = 150$ (b) Ringing vs L_c

Fig. 7. (a) Combined frequency response of a 4-scale wavelet filter bank obtained by our optimization procedure. $a = \{4, 2, 1, 0.5\}$. Invertibility is imposed from degree 10 to 89. Combined frequency response cutoff is set to $L_c = 150$. (b) Plot of ringing versus cutoff frequency L_c.

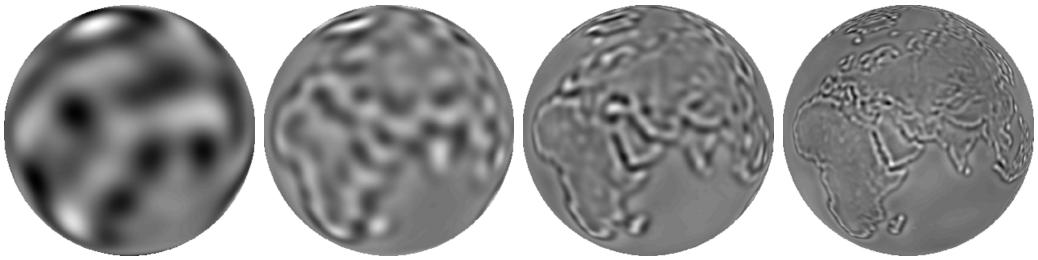

(a) a = 4 (b) a = 2 (c) a = 1 (d) a = 0.5

Fig. 8. Convolution outputs obtained by applying the analysis filter bank of Figure 7(a) to the world elevation map of Figure 6(a). Notice that there is less ringing artifacts than in Figure 6 because ringing is lower in the 4-scale filter bank than in the 10-scale filter bank when L_c is set to 150.

B. Spherical Steerable Pyramid

Just like the Euclidean domain [12], it can be shown that there is a direct tradeoff between angular resolution and steerability of oriented (axis-asymmetric) filters on the sphere [25], i.e., filters that have higher angular resolving power requires a bigger set of "steering" basis filters.

In our experiments, we limit our set of basis functions $\{B^i\}$ to be the first two hundred spherical harmonics of order $+1$ and -1. We note that we can increase our angular power by using higher orders, but this decreases the steerability of our filters. By considering only real filters, we can avoid working directly with the order -1 spherical harmonics, since their coefficients are effectively constrained by those of the order $+1$ spherical harmonics (see Appendix A). For convenience, we further assume that

the coefficients of the order $+1$ spherical harmonics are real.

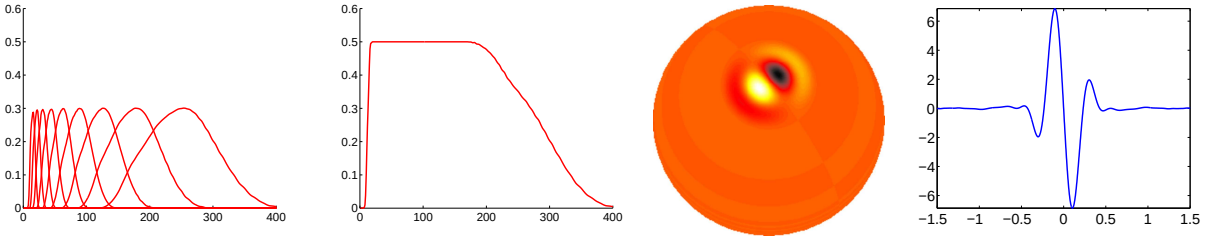

(a) Individual frequency response (b) Combined frequency response (c) $h_{a=4}(\theta,\phi)$ (d) Plot of $h_{a=4}(\theta,\phi)$ ($-1.5 \leq \theta \leq 1.5$ radian)

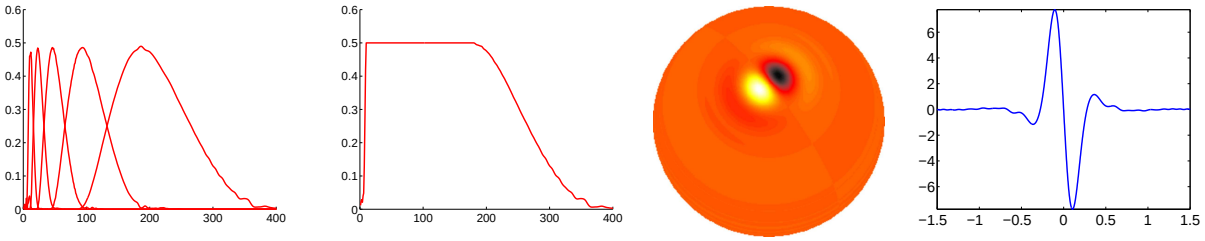

(e) Individual frequency response (f) Combined frequency response (g) $h_{a=4}(\theta,\phi)$ (h) Plot of $h_{a=4}(\theta,\phi)$ ($-1.5 \leq \theta \leq 1.5$ radian)

Fig. 9. (a-d) Illustrates the 9-scale steerable pyramid ($a = \{2^{-\frac{n}{2}}\}, n = -4, \cdots, 4$) obtained by imposing invertibility from degree 20 to 170. Note that the frequency response is equal to 0.5 in the invertibility range because we only plot the frequency response contributed by the order $+1$ harmonics. (e-h) Illustrates the 5-scale steerable pyramid ($a = \{4, 2, 1, 0.5, 0.25\}$) obtained by imposing invertibility from degree 10 to 180. Note that the frequency response is equal to 0.5 in the invertibility range because we only plot the frequency response contributed by the order $+1$ harmonics.

We define the set of scales to be $a = \{2^{-\frac{n}{2}}\}, n = -4, \cdots, 4$, with $a = 1$ corresponding to the undilated template. Once again, we use S2kit [13] to create a table of the spherical harmonic coefficients of $D_a Y_l^1$ for $l = 1, \cdots, 200$. We find the first 999 order 1 spherical harmonic coefficient of each dilated spherical harmonic (the order of a spherical function does not change under dilation). We verify that for $a = 4$ and $a = 0.25$, $[D_a Y_{200}^1]^{999,1} < 10^{-7}$.

Similar to the previous subsection, we penalize the magnitude of the leading coefficients of $h_{a=1}(\theta,\phi)$. We also penalize the second derivatives of the filters' frequency responses and spherical harmonic coefficients. Finally, we fix the amplitude scaling factors b_k's at all scales to be the same.

Figure 9(a-b) illustrates the frequency response of a 9-scale steerable pyramid ($a = \{2^{-\frac{n}{2}}\}, n = -4, \cdots, 4$) obtained through our optimization procedure. Invertibility is enforced from degree 20 to

170. Note that the frequency response is equal to 0.5 in the invertibility range because we only plot the frequency response contributed by the order $+1$ harmonics. Figure 9(c) shows $h_{a=4}(\theta, \phi)$ as a spherical image. Note that it looks like a derivative of gaussian. We can also to quantify ringing by plotting $h_{a=4}(\theta, \phi)$ as a function of θ while fixing ϕ to correspond to the great circle passing through the maxima and minima of the filter (Figure 9(d)).

Similarly, Figure 9(e-f) shows the frequency response of a 5-scale steerable pyramid ($a = \{4, 2, 1, 0.5, 0.25\}$) obtained through our optimization procedure. Invertibility is enforced from degree 10 to 180. Figure 9(g) shows $h_{a=4}(\theta, \phi)$ as a spherical image and Figure 9(h) is a plot of $h_{a=4}(\theta, \phi)$ as a function of θ by fixing ϕ.

VII. Discussion and Conclusion

In this paper, we present the theoretical conditions for the invertibility of filter banks under continuous convolution on the 2-Sphere. We discretize the results using quadrature, thus obtaining a generalized sampling theorem. We propose a general procedure for constructing invertible filter banks and demonstrate the procedure by generating self-invertible spherical wavelets and steerable pyramids.

Nonlinear dilation of functions on the sphere remains difficult to work with. While we circumvent the problem by using the distributive property of stereographic dilation, the spherical harmonic coefficients table can take up a substantial amount of space. More efficient methods are therefore needed. It might also be possible to formulate other definitions of dilation that fit better into the computational framework.

More work is needed to understand the space of invertible and self-invertible filter banks. As we saw in our experiments, there is an implicit tradeoff between the sharpness of the frequency response of the filters and ringing. It will be useful to formulate an objective function that directly trades off between ringing and the sharpness of the frequency response.

This paper introduces theoretical results on invertibility and sampling, and represents a step towards a general framework for filter design on the 2-Sphere. Just as wavelets and steerable pyramids have been useful for the processing and analysis of planar images, we are optimistic that future work will lead to similar applications on the sphere.

Appendix A
Spherical Harmonics Basics

Here we review useful facts on the spherical harmonics.

A. Spherical Harmonics

The spherical harmonics Y_l^m are defined in terms of the associated Legendre polynomials P_l^m. For a given degree $l \geq 0$ and order $|m| \leq l$, $0 \leq \theta \leq \pi$ and $0 \leq \phi \leq 2\pi$

$$Y_l^m(\theta,\phi) = \sqrt{\frac{2l+1}{4\pi}\frac{(l-m)!}{(l+m)!}}P_l^m(\cos\theta)e^{im\phi} \tag{18}$$

where, for $m \geq 0$ and $|x| < 1$,

$$P_l^m(x) = \frac{(-1)^m}{2^l l!}(1-x^2)^{m/2}\frac{d^{l+m}}{dx^{l+m}}(x^2-1)^l \tag{19}$$

$$P_l^{-m}(x) = (-1)^m\frac{(l-m)!}{(l+m)!}P_l^m(x) \tag{20}$$

Therefore, for $l \geq m \geq 0$, we have,

$$Y_l^m(\theta,\phi) = \sqrt{\frac{2l+1}{4\pi}\frac{(l-m)!}{(l+m)!}}\frac{(-1)^m}{2^l l!}(1-\cos^2\theta)^{m/2}\frac{d^{l+m}}{dx^{l+m}}(x^2-1)^l\Big|_{x=\cos\theta}e^{im\phi} \tag{21}$$

$$Y_l^{-m}(\theta,\phi) = \sqrt{\frac{2l+1}{4\pi}\frac{(l-m)!}{(l+m)!}}\frac{1}{2^l l!}(1-\cos^2\theta)^{m/2}\frac{d^{l+m}}{dx^{l+m}}(x^2-1)^l\Big|_{x=\cos\theta}e^{-im\phi} \tag{22}$$

$$= (-1)^m Y_l^{m*}(\theta,\phi) \tag{23}$$

B. Rotation of Spherical Harmonics on the Sphere

Under rotation, each spherical harmonic of degree l is transformed into a linear combination of spherical harmonics of the same degree but possibly different orders. In particular if we parametrize our rotation by the three Euler angles, α, β, γ, and rotate our original function f, it can be shown that:

$$[D(\alpha,\beta,\gamma)f]^{l,m} = \sum_{m'=-l}^{l} D^l_{mm'}(\alpha,\beta,\gamma)f^{l,m'} \tag{24}$$

where $D^l_{mm'}(\alpha,\beta,\gamma)$ is the Wigner-D function [17]. We can further decompose $D^l_{mm'}(\alpha,\beta,\gamma)$ as follows:

$$D^l_{mm'}(\alpha,\beta,\gamma) = e^{-im\alpha}d^l_{mm'}(\beta)e^{-im'\gamma} \tag{25}$$

where $d^l_{mm'}(\beta)$ is the Wigner-d function and is real [17]:

$$d^l_{mm'}(\beta) = \sum_j (-1)^{j-m'+m}\frac{\sqrt{(l+m')!(l-m')!(l+m)!(l-m)!}}{(l+m'-j)!j!(l-j-m)!(j-m'+m)!} (\cos\frac{\beta}{2})^{2l-2j+m'-m}(\sin\frac{\beta}{2})^{2j-m'+m} \tag{26}$$

The sum is over all j such that none of the denominator terms with factorials is negative. This reflects the fact that only rotations about the y-axis mixes orders.

By the Peter-Weyl theorem on compact groups [26]

$$\int_{SO(3)} D^l_{mn}(\rho) D^{l'*}_{m'n'}(\rho) d\rho = \frac{8\pi^2}{2l+1}\delta(l-l', m-m', n-n') \tag{27}$$

By integrating out α and γ, we obtain

$$\int_\beta d^l_{mn}(\beta) d^{l'}_{mn}(\beta) \sin\beta d\beta = \frac{2}{2l+1}\delta(l-l') \tag{28}$$

We will also use the following identity which algebraically relates spherical harmonics and the wigner-D functions.

$$Y^m_l(\beta,\alpha) = \sqrt{\frac{2l+1}{4\pi}}\Big[D^l_{m0}(\alpha,\beta,\gamma)\Big]^* = \sqrt{\frac{2l+1}{4\pi}}\Big[e^{-im\alpha} d^l_{m0}(\beta)\Big]^* \quad \text{for any} \quad \gamma \tag{29}$$

APPENDIX B
PROOF OF CONTINUOUS-INVERTIBILITY

Here, we prove Theorem 4.1 on continuous frequency response. We first note that by using Parseval's Theorem and substituting Eq. (24), we can re-write the output of the n-th analysis filter as

$$y_n(\alpha,\beta,\gamma) = \int_{S^2} [D(\alpha,\beta,\gamma)\widetilde{h}_n]^*(\theta,\phi) x(\theta,\phi) d\Omega \tag{30}$$

$$= \sum_{l'=0}^{\infty}\sum_{m'=-l'}^{l'}\left[\sum_{m''=-l'}^{l'} D^{l'}_{m',m''}(\alpha,\beta,\gamma)\widetilde{h}^{l',m''}_n\right]^* x^{l',m'} \tag{31}$$

and the reconstructed image as

$$\widehat{x}(\theta,\phi) = \sum_{n=1}^{N}\int_{SO(3)} [D(\alpha,\beta,\gamma)h_n](\theta,\phi) y_n(\alpha,\beta,\gamma) d\rho \tag{32}$$

$$\overset{(31)}{=} \sum_{n=1}^{N}\int_{SO(3)} [D(\alpha,\beta,\gamma)h_n](\theta,\phi) \sum_{l'=0}^{\infty}\sum_{m'=-l'}^{l'}\left[\sum_{m''=-l'}^{l'} D^{l'}_{m',m''}(\alpha,\beta,\gamma)\widetilde{h}^{l',m''}_n\right]^* x^{l',m'} d\rho \tag{33}$$

Projecting $\widehat{x}(\theta,\phi)$ onto the spherical harmonics basis we obtain

$$\widehat{x}^{l,m} = \int_{S^2} \widehat{x}(\theta,\phi) Y^{m*}_l(\theta,\phi) d\Omega \tag{34}$$

$$\overset{(33)}{=} \sum_{n=1}^{N}\int_{SO(3)}\Big[\int_{S^2} [D(\alpha,\beta,\gamma)h_n](\theta,\phi) Y^{m*}_l(\theta,\phi) d\Omega\Big] \sum_{l'=0}^{\infty}\sum_{m'=-l'}^{l'}\left[\sum_{m''=-l'}^{l'} D^{l'}_{m',m''}(\alpha,\beta,\gamma)\widetilde{h}^{l',m''}_n\right]^* x^{l',m'} d\rho \tag{35}$$

$$\overset{(24)}{=} \sum_{n=1}^{N}\int_{SO(3)}\left[\sum_{m'''=-l}^{l} h^{l,m'''}_n D^l_{m,m'''}(\alpha,\beta,\gamma)\right] \sum_{l'=0}^{\infty}\sum_{m'=-l'}^{l'}\left[\sum_{m''=-l'}^{l'} D^{l'}_{m',m''}(\alpha,\beta,\gamma)\widetilde{h}^{l',m''}_n\right]^* x^{l',m'} d\rho \tag{36}$$

$$= \sum_{n=1}^{N}\sum_{m'''=-l}^{l}\left[h^{l,m'''}_n\right] \sum_{l'=0}^{\infty}\sum_{m'=-l'}^{l'} x^{l',m'} \sum_{m''=-l'}^{l'}\left[\widetilde{h}^{l',m''}_n\right]^* \int_{SO(3)} D^l_{m,m'''}(\alpha,\beta,\gamma) D^{l'}_{m',m''}(\alpha,\beta,\gamma)^* d\rho \tag{37}$$

$$\overset{(27)}{=} x^{l,m}\frac{8\pi^2}{2l+1}\Big\{\sum_{n=1}^{N}\sum_{m'''=-l}^{l}\left[h^{l,m'''}_n\right]\left[\widetilde{h}^{l,m'''}_n\right]^*\Big\} \tag{38}$$

APPENDIX C
PROOF OF DISCRETE-INVERTIBILITY

Here, we prove the generalized sampling theorem. Recall from section III that $y_n(\alpha_{j,n}, \beta_{s,n}, \gamma_{k,n})$ are samples of $y_n(\alpha, \beta, \gamma)$. Recall also that we define $\widetilde{L}_n = \min(L, L_{\widetilde{h}_n})$. Therefore, from Eq. (31) and noting that the maximum degree of x is L ($L < \infty$), we get

$$y_n(\alpha_{j,n}, \beta_{s,n}, \gamma_{k,n}) = \sum_{l'=0}^{\widetilde{L}_n} \sum_{m'=-l'}^{l'} \left[\sum_{m''=-l'}^{l'} D^{l'}_{m',m''}(\alpha_{j,n}, \beta_{s,n}, \gamma_{k,n}) \widetilde{h}_n^{l',m''} \right]^* x^{l',m'} \tag{39}$$

For $w_{j,s,k,n} = \frac{4\pi^2 w_{s,n}}{J_n K_n}$ (as required by the theorem), the output of the n-th synthesis filter becomes

$$\widehat{x}_n(\theta,\phi) = \sum_{j=0}^{J_n-1} \sum_{s=0}^{S_n-1} \sum_{k=0}^{K_n-1} w_{j,s,k,n} [D(\alpha_{j,n}, \beta_{s,n}, \gamma_{k,n}) h_n](\theta,\phi) y_n(\alpha_{j,n}, \beta_{s,n}, \gamma_{k,n}) \tag{40}$$

$$\stackrel{(39)}{=} \sum_{j=0}^{J_n-1} \sum_{s=0}^{S_n-1} \sum_{k=0}^{K_n-1} \frac{4\pi^2 w_{s,n}}{J_n K_n} [D(\alpha_{j,n}, \beta_{s,n}, \gamma_{k,n}) h_n](\theta,\phi) \tag{41}$$

$$\sum_{l'=0}^{\widetilde{L}_n} \sum_{m'=-l'}^{l'} \left[\sum_{m''=-l'}^{l'} D^{l'}_{m',m''}(\alpha_{j,n}, \beta_{s,n}, \gamma_{k,n}) \widetilde{h}_n^{l',m''} \right]^* x^{l',m'}$$

Projecting $\widehat{x}_n(\theta,\phi)$ onto the spherical harmonics, for $l \leq L$ (and thus $|m| \leq L$), we have

$$\widehat{x}_n^{l,m} = \int_{S^2} \widehat{x}_n(\theta,\phi) Y_l^{m*}(\theta,\phi) d\Omega$$

$$\stackrel{(24)}{=} \sum_{j=0}^{J_n-1} \sum_{s=0}^{S_n-1} \sum_{k=0}^{K_n-1} \frac{4\pi^2 w_{s,n}}{J_n K_n} \left[\sum_{m'''=-l}^{l} D^{l}_{m,m'''}(\alpha_{j,n}, \beta_{s,n}, \gamma_{k,n}) h_n^{l,m'''} \right] \tag{42}$$

$$\sum_{l'=0}^{\widetilde{L}_n} \sum_{m'=-l'}^{l'} \left[\sum_{m''=-l'}^{l'} D^{l'}_{m',m''}(\alpha_{j,n}, \beta_{s,n}, \gamma_{k,n}) \widetilde{h}_n^{l',m''} \right]^* x^{l',m'}$$

$$= \frac{4\pi^2}{J_n K_n} \sum_{m'''=-l}^{l} h_n^{l,m'''} \sum_{l'=0}^{\widetilde{L}_n} \sum_{m'=-l'}^{l'} x^{l',m'} \sum_{m''=-l'}^{l'} \left[\widetilde{h}_n^{l',m''} \right]^* \tag{43}$$

$$\sum_{j=0}^{J_n-1} \sum_{s=0}^{S_n-1} \sum_{k=0}^{K_n-1} w_{s,n} D^{l}_{m,m'''}(\alpha_{j,n}, \beta_{s,n}, \gamma_{k,n}) D^{l'*}_{m',m''}(\alpha_{j,n}, \beta_{s,n}, \gamma_{k,n})$$

where we have arranged the terms so that they look like the setup for Peter-Weyl Theorem, except we have summations instead of integrals. Let Φ be the last part of Eq. (43), and thus we have

$$\widehat{x}_n^{l,m} = \frac{4\pi^2}{J_n K_n} \sum_{m'''=-l}^{l} h_n^{l,m'''} \sum_{l'=0}^{\widetilde{L}_n} \sum_{m'=-l'}^{l'} x^{l',m'} \sum_{m''=-l'}^{l'} \left[\widetilde{h}_n^{l',m''} \right]^* \Phi \tag{44}$$

To simplify Φ, we write

$$\Phi = \sum_{j=0}^{J_n-1}\sum_{s=0}^{S_n-1}\sum_{k=0}^{K_n-1} w_{s,n} D^l_{m,m'''}(\alpha_{j,n},\beta_{s,n},\gamma_{k,n}) D^{l'*}_{m',m''}(\alpha_{j,n},\beta_{s,n},\gamma_{k,n}) \quad (45)$$

$$\stackrel{(25)}{=} \sum_{j=0}^{J_n-1}\sum_{s=0}^{S_n-1}\sum_{k=0}^{K_n-1} w_{s,n} e^{-im\alpha_{j,n}} d^l_{m,m'''}(\beta_{s,n}) e^{-im'''\gamma_{k,n}} e^{im'\alpha_{j,n}} d^{l'}_{m',m''}(\beta_{s,n}) e^{im''\gamma_{k,n}} \quad (46)$$

$$= \sum_{s=0}^{S_n-1} w_{s,n} d^l_{m,m'''}(\beta_{s,n}) d^{l'}_{m',m''}(\beta_{s,n}) \left[\sum_{j=0}^{J_n-1} e^{i(m'-m)\alpha_{j,n}}\right]\left[\sum_{k=0}^{K_n-1} e^{i(m''-m''')\gamma_{k,n}}\right] \quad (47)$$

We note that $|m'| \le l' \le \widetilde{L}_n$ and $|m| \le L$, and therefore $-\widetilde{L}_n - L \le m' - m \le \widetilde{L}_n + L$. Since $\alpha_{j,n} = \frac{2\pi j}{\widetilde{L}_n+L+1}$, $j = 0, 1, \cdots, \widetilde{L}_n + L$, we can conclude via the geometric series that

$$\sum_{j=0}^{J_n-1} e^{i(m'-m)\alpha_{j,n}} = \sum_{j=0}^{\widetilde{L}_n+L} e^{i(m'-m)\frac{2\pi j}{\widetilde{L}_n+L+1}} = \begin{cases} \widetilde{L}_n + L + 1 & \text{if } (m'-m) = 0 \\ 0 & \text{otherwise} \end{cases} \quad (48)$$

Similarly, from Eq. (42), we observe that $|m''| \le O_{\widetilde{h}_n}$ and $|m'''| \le O_{h_n}$. Using the same reasoning, we get

$$\sum_{k=0}^{K_n-1} e^{i(m''-m''')\gamma_{k,n}} = \sum_{k=0}^{O_{\widetilde{h}_n}+O_{h_n}} e^{i(m''-m''')\frac{2\pi k}{O_{\widetilde{h}_n}+O_{h_n}+1}} = \begin{cases} O_{\widetilde{h}_n} + O_{h_n} + 1 & \text{if } (m''-m''') = 0 \\ 0 & \text{otherwise} \end{cases} \quad (49)$$

Substituting into Eq. (47), we get

$$\Phi = \sum_{s=0}^{S_n-1} w_{s,n} d^l_{m,m'''}(\beta_{s,n}) d^{l'}_{m',m''}(\beta_{s,n}) \left[\sum_{j=0}^{J_n-1} e^{i(m'-m)\alpha_{j,n}}\right]\left[\sum_{k=0}^{K_n-1} e^{i(m''-m''')\gamma_{k,n}}\right] \quad (50)$$

$$= J_n K_n \sum_{s=0}^{S_n-1} w_{s,n} d^l_{m,m'''}(\beta_{s,n}) d^{l'}_{m',m''}(\beta_{s,n}) \delta(m-m')\delta(m''-m''') \quad (51)$$

$$= J_n K_n \sum_{s=0}^{S_n-1} w_{s,n} d^l_{m,m''}(\beta_{s,n}) d^{l'}_{m,m''}(\beta_{s,n}) \delta(m-m')\delta(m''-m''') \quad (52)$$

$$\stackrel{(28)}{=} \frac{2J_nK_n}{2l+1}\delta(l-l')\delta(m-m')\delta(m''-m''') \quad (53)$$

where in the third equality, $m''' = m'', m' = m$ because of the delta functions, and the last equality was obtained using the assumption that $w_{s,n}$ and $\beta_{s,n}$ are the quadrature weights and knots of the integral

$\int_0^\pi d^l_{mm''}(\beta)d^{l'}_{mm''}(\beta)\sin(\beta)d\beta$. We can now substitute Eq. (53) back into Eq. (44):

$$\begin{aligned}
&\widehat{x}_n^{l,m} \\
&= \frac{4\pi^2}{J_nK_n}\sum_{m'''=-l}^{l} h_n^{l,m'''}\sum_{l'=0}^{\widetilde{L}_n}\sum_{m'=-l'}^{l'} x^{l',m'}\sum_{m''=-l'}^{l'}\left[\widetilde{h}_n^{l',m''}\right]^*\Phi && (54)\\
&= \frac{4\pi^2}{J_nK_n}\sum_{m'''=-l}^{l} h_n^{l,m'''}\sum_{l'=0}^{\widetilde{L}_n}\sum_{m'=-l'}^{l'} x^{l',m'}\sum_{m''=-l'}^{l'}\left[\widetilde{h}_n^{l',m''}\right]^*\frac{2J_nK_n}{2l+1}\delta(l-l')\delta(m-m')\delta(m''-m''') && (55)\\
&= \frac{8\pi^2}{2l+1}x^{l,m}\sum_{m''=-l}^{l} h_n^{l,m''}\widetilde{h}_n^{l,m''*} && (56)
\end{aligned}$$

Noting that $\widehat{x}(\theta,\phi)=\sum_{n=1}^N \widehat{x}_n(\theta,\phi)$, we have

$$\widehat{x}^{l,m}=\sum_{n=1}^{N}\widehat{x}_n^{l,m}=\frac{8\pi^2}{2l+1}x^{l,m}\sum_{n=1}^{N}\sum_{m''=-l}^{l}h_n^{l,m''}\widetilde{h}_n^{l,m''*}=x^{l,m}\quad\text{for all } 0\le l\le L \tag{57}$$

APPENDIX D
QUADRATURE RULES

In this appendix, we derive two different quadrature rules that satisfy the conditions of Theorem 4.3, namely, we show quadrature weights $w_{s,n}$ and knots $\beta_{s,n}$, such that for $l\le L, l'\le\widetilde{L}_n$,

$$\int_0^\pi d^l_{mm'}(\beta)d^{l'}_{mm'}(\beta)\sin(\beta)d\beta=\sum_{s=0}^{S_n-1}w_{s,n}d^l_{mm'}(\beta_{s,n})d^{l'}_{mm'}(\beta_{s,n}) \tag{58}$$

A. Quadrature Rule (1)

We denote $f(\beta)=d^l_{mm'}(\beta)d^{l'}_{mm'}(\beta)$ and observe that $f(\beta)$ consists of a linear combination of even powers of $\cos(\beta/2)$ and $\sin(\beta/2)$ (see Eq. (26)). Therefore, if we make the substitution $u=\sin(\beta/2)$, and noting that $f(u)$ (where we are overloading f) is now a polynomial with maximum degree, $Q=2(l+l')\le 2(L+\widetilde{L}_n)$, we get

$$\int_0^\pi f(\beta)\sin\beta d\beta=2\int_0^\pi f(\beta)\sin(\beta/2)\cos(\beta/2)d\beta=4\int_0^1 f(u)udu \tag{59}$$

Now, making the substitution, $v=2u-1$, we have

$$\int_0^\pi f(\beta)\sin\beta d\beta=2\int_{-1}^1 f\left(\frac{v+1}{2}\right)\frac{v+1}{2}dv=2\sum_{k=0}^{N-1}r_k\frac{v_k+1}{2}f\left(\frac{v_k+1}{2}\right) \tag{60}$$

where r_k's are defined to be the weights of the Gauss-Legendre quadrature on the interval $[-1,1]$, and v_k's correspond to the sampling knots [16]. The weights and abscissas can be found by standard algorithms (see for example [16]). In general, quadrature integration is exact up to polynomial powers $2N-1$ where

N is the number of samples. Because the integrand's highest polynomial power is $Q+1$, if $N \geq \frac{Q}{2}+1$ (or $N \geq \lceil \frac{Q}{2} \rceil + 1$), then $2N-1 \geq Q+1$ and thus the quadrature formula is exact.

From the substitution above, we have $\sin\frac{\beta_k}{2} = u_k = \frac{v_k+1}{2}$ or $\beta_k = 2\sin^{-1}(\frac{v_k+1}{2})$. In conclusion, for $N = \lceil \frac{Q}{2} \rceil + 1$, we have $\int_0^\pi d^l_{mm'}(\beta) d^{l'}_{mm'}(\beta) \sin\beta d\beta = \sum_{s=0}^{N-1} w_s f(\beta_s)$, $w_s = r_s(v_s+1)$ and $\beta_s = 2\sin^{-1}(\frac{v_s+1}{2})$, where r_s and v_s are the quadrature weights and knots of the Gauss-Legendre quadrature.

B. Quadrature Rule 2

We will derive another rule in this section, using the technique shown in [9]. But first we need to obtain the fourier series formula for the square wave, $SQ(u)$, which is defined to be periodic from $-\pi$ to π,

$$SQ(u) = \begin{cases} 1 & -\pi < u < -\pi/2 \\ -1 & -\pi/2 < u < 0 \\ 1 & 0 < u < \pi/2 \\ -1 & \pi/2 < u < \pi \end{cases} \tag{61}$$

Projecting $SQ(u)$ onto the fourier series basis, we get

$$\begin{aligned} \frac{1}{2\pi}\int_{-\pi}^{\pi} SQ(u)e^{-iku}du &= \frac{1}{2\pi}\left[\int_{-\pi}^{-\pi/2} e^{-iku}du - \int_{-\pi/2}^{0} e^{-iku}du + \int_{0}^{\pi/2} e^{-iku}du - \int_{\pi/2}^{\pi} e^{-iku}du\right] && (62)\\ &= \frac{i}{2\pi k}\left[e^{-iku}\Big|_{-\pi}^{-\pi/2} - e^{-iku}\Big|_{-\pi/2}^{0} + e^{-iku}\Big|_{0}^{\pi/2} - e^{-iku}\Big|_{\pi/2}^{\pi}\right] && (63)\\ &= \frac{i}{2\pi k}\left[(e^{ik\frac{\pi}{2}} - e^{ik\pi}) - (1 - e^{ik\frac{\pi}{2}}) + (e^{-ik\frac{\pi}{2}} - 1) - (e^{-ik\pi} - e^{-ik\frac{\pi}{2}})\right] && (64)\\ &= \frac{i}{\pi k}\left[e^{ik\frac{\pi}{2}} + e^{-ik\frac{\pi}{2}} - 1 - \frac{1}{2}e^{ik\pi} - \frac{1}{2}e^{-ik\pi}\right] && (65)\\ &= \frac{i}{\pi k}\left[2\cos(k\frac{\pi}{2}) - 1 - \cos(k\pi)\right] && (66) \end{aligned}$$

If $k = 4n$, we get $2\cos(2n\pi) - 1 - \cos(4n\pi) = 0$

If $k = 4n+1$, we get $2\cos(2n\pi + \frac{\pi}{2}) - 1 - \cos(4n\pi + \pi) = 0$

If $k = 4n+2$, we get $2\cos(2n\pi + \pi) - 1 - \cos(4n\pi + 2\pi) = -4$

If $k = 4n+3$, we get $2\cos(2n\pi + \frac{3\pi}{2}) - 1 - \cos(4n\pi + 3\pi) = 0$

Therefore, the fourier series for $SQ(u)$ is non-zero for $k = 4n+2$, and is equal to $-4\frac{i}{\pi k}$, and we have

$$SQ(u) = \sum_{p=-\infty}^{\infty} -\frac{4i}{\pi(4p+2)}e^{i(4p+2)u} = \sum_{p=-\infty}^{\infty} -\frac{2i}{\pi(2p+1)}e^{i(4p+2)u} \tag{67}$$

Now, we can continue with the derivation of the quadrature. We note that $f(\beta) = \sum_{k,k'} a_k \cos(\beta/2)^k \sin(\beta/2)^{k'}$, where k and k' are always even, non-negative and bounded (once again, we are overloading f). We can

express them as complex exponentials so that $f(\beta) = \sum_q b_q (e^{i\beta/2})^q$ where q can take on negative values, but it is still bounded: $|q| \leq 2(l+l') \leq 2(L+\widetilde{L}_n)$. Note that if we make the substitution $\beta' = \beta/2$, we now have $f(\beta') = \sum_{k,k'} a_k \cos(\beta')^k \sin(\beta')^{k'} = \sum_q b_q (e^{i\beta'})^q$. Therefore,

$$\begin{aligned}
\int_0^\pi f(\beta)\sin(\beta)d\beta &= 2\int_0^{\pi/2} f(\beta')\sin(2\beta')d\beta' && (68)\\
&= \frac{1}{2}\int_{-\pi}^{-\pi/2} f(\beta')\sin(2\beta')d\beta' - \frac{1}{2}\int_{-\pi/2}^{0} f(\beta')\sin(2\beta')d\beta' && (69)\\
&\qquad + \frac{1}{2}\int_0^{\pi/2} f(\beta')\sin(2\beta')d\beta' - \frac{1}{2}\int_{\pi/2}^{\pi} f(\beta')\sin(2\beta')d\beta'\\
&= \frac{1}{2}\int_{-\pi}^{\pi} f(\beta')\sin(2\beta')SQ(\beta')d\beta' && (70)
\end{aligned}$$

where the middle equality was obtained using symmetry arguments since f is a linear combination of even positive powers of $\sin$ and $\cos$.

Since $|q| \leq Q$ implies that the term $f(\beta')\sin(2\beta')$ has exponential powers $\leq Q+2$, we can eliminate terms in the fourier series of $SQ(\beta')$ that falls out of the range (by orthonormality of the exponentials), thus we only require p such that

$$\begin{aligned}
& |4p+2| \leq Q+2 && (71)\\
\Leftrightarrow\quad & -Q-2 \leq 4p+2 \leq Q+2 && (72)\\
\Leftrightarrow\quad & -\frac{Q}{4} - 1 \leq p \leq \frac{Q}{4} && (73)\\
\Leftrightarrow\quad & -\lfloor\frac{Q}{4}\rfloor - 1 \leq p \leq \lfloor\frac{Q}{4}\rfloor && (74)
\end{aligned}$$

Defining $\widetilde{SQ}(\beta') = \sum_{p=-\lfloor\frac{Q}{4}\rfloor-1}^{\lfloor\frac{Q}{4}\rfloor} -\frac{2i}{\pi(2p+1)} e^{i(4p+2)\beta'}$, we have

$$\begin{aligned}
\int_0^\pi f(\beta)\sin(\beta)d\beta &= \frac{1}{2}\int_{-\pi}^{\pi} f(\beta')\sin(2\beta')\widetilde{SQ}(\beta')d\beta' && (75)\\
&= \frac{1}{2}\sum_{q=-Q}^{Q} b_q \sum_{p=-\lfloor\frac{Q}{4}\rfloor-1}^{\lfloor\frac{Q}{4}\rfloor} -\frac{2i}{\pi(2p+1)}\int_{-\pi}^{\pi} e^{i\beta' q}\frac{e^{i2\beta'} - e^{-i2\beta'}}{2i} e^{i(4p+2)\beta'}d\beta' && (76)
\end{aligned}$$

Let us define the highest exponential power to be B and notice that $B = Q+2+4\lfloor\frac{Q}{4}\rfloor+2 = Q+4\lfloor Q/4\rfloor+4$, while lowest exponential power corresponds to $-Q-2-4\lfloor\frac{Q}{4}\rfloor-2 = -Q-4\lfloor\frac{Q}{4}\rfloor-4 = -B$. Let N be the smallest integer such that $B < 4N$, where N is an integer. Therefore, $N = \lfloor\frac{Q}{4}\rfloor+\lfloor\frac{Q}{4}\rfloor+1+1 = 2\lfloor\frac{Q}{4}\rfloor+2$

It is easy to verify the following identity:

$$\frac{1}{4N}\sum_{k=-2N}^{2N-1} e^{\frac{2\pi i k l}{4N}} = \frac{1}{2\pi}\int_{-\pi}^{\pi} e^{il\beta'}d\beta' = \begin{cases} 1 & \text{if } l=0 \\ 0 & \text{otherwise} \end{cases} \qquad \forall |l| < 4N \qquad (77)$$

Substituting the identity into Eq. (76), we get ($\beta' \to \frac{2\pi k}{4N}$),

$$\begin{aligned}
&\frac{1}{2}\sum_{q=-Q}^{Q} b_q \sum_{p=-\lfloor\frac{Q}{4}\rfloor-1}^{\lfloor\frac{Q}{4}\rfloor} -\frac{2i}{\pi(2p+1)}\frac{\pi}{2N}\sum_{k=-2N}^{2N-1} e^{\frac{2\pi ikq}{4N}}\frac{e^{\frac{2\pi ik2}{4N}}-e^{\frac{-2\pi ik2}{4N}}}{2i}e^{\frac{2\pi ik(4p+2)}{4N}} \\
&= \frac{\pi}{4N}\sum_{k=-2N}^{2N-1}\sum_{q=-Q}^{Q} b_q e^{\frac{2\pi ikq}{4N}}\sin(\frac{4\pi k}{4N})\sum_{p=-\lfloor\frac{Q}{4}\rfloor-1}^{\lfloor\frac{Q}{4}\rfloor} -\frac{2i}{\pi(2p+1)}e^{\frac{2\pi ik(4p+2)}{4N}} && (78)\\
&= \frac{\pi}{4N}\sum_{k=-2N}^{2N-1} f(\beta'_k=\frac{2\pi k}{4N})\sin(\frac{4\pi k}{4N})\widetilde{SQ}(\frac{2\pi k}{4N}) && (79)\\
&= \frac{\pi}{4N}\sum_{k=-2N}^{2N-1} f(\beta'_k=\frac{2\pi k}{4N})\sin(\frac{\pi k}{N})\widetilde{SQ}(\frac{\pi k}{2N}) && (80)\\
&= \frac{\pi}{2N}\sum_{k=0}^{2N-1} f(\beta'_k=\frac{2\pi k}{4N})\sin(\frac{\pi k}{N})\widetilde{SQ}(\frac{\pi k}{2N}) && (81)\\
&= \frac{\pi}{N}\sum_{k=0}^{N-1} f(\beta'_k=\frac{2\pi k}{4N})\sin(\frac{\pi k}{N})\widetilde{SQ}(\frac{\pi k}{2N}) && (82)
\end{aligned}$$

where the second last equality uses the fact that $\sin(-2\pi) = 0$ and the function f is even, and the last equality uses the fact that $\sin\pi = 0$ and $f(\beta')$ is even about $\beta' = \pi$. Because $\beta'_k = \beta_k/2 = \frac{2\pi k}{4N}$, hence $\beta_k = \frac{\pi k}{N}$ for $k = 0, 1, \cdots N-1$ corresponds to our quadrature knots, with quadrature weights, $w_k = \frac{\pi}{N}\sin(\frac{\pi k}{N})\widetilde{SQ}(\frac{\pi k}{2N})$.

C. Summary

We have formulated two possible ways of obtaining an exact quadrature of $\int_0^\pi d^l_{mm'}(\beta)d^{l'}_{mm'}(\beta)d\beta$ and the integral is equal to $\sum_{s=0}^{N-1} w_s d^l_{mm'}(\beta_s)d^{l'}_{mm'}(\beta_s) = \frac{2}{2l+1}\delta(l-l')$ if we select the correct samples and corresponding weights. In particular, this is true for

1) $\beta_s = 2\sin^{-1}(\frac{v_s+1}{2})$ and $w_s = r_s(v_s+1)$, $s = 0, 1, \cdots N-1$, where
   a) $N = \lceil\frac{Q}{2}\rceil + 1$
   b) Q is the highest power of $d^l_{mm'}(\beta)d^{l'}_{mm'}(\beta)$ when viewed as a polynomial in $\sin\frac{\beta}{2}$
   c) r_s and v_s are the weights and nodes of the Gaussian-Lengendre quadrature on the interval [-1,1]
2) $\beta_s = \frac{\pi s}{N}$ and $w_s = \frac{\pi}{N}\sin(\frac{\pi s}{N})\widetilde{SQ}(\frac{\pi s}{2N})$, $s = 0, 1, \cdots N-1$, where
   a) $N = 2\lfloor\frac{Q}{4}\rfloor + 2$,
   b) Q is the highest power of $d^l_{mm'}(\beta)d^{l'}_{mm'}(\beta)$ when viewed as a polynomial in $e^{i\frac{\beta}{2}}$

Note that $Q = 2(l+l') \le 2(L+\widetilde{L}_n)$

APPENDIX E
INVERSE CONVOLUTION WITH AXIS-SYMMETRIC FILTER

Here, we illustrate the computation of the inverse convolution of $y(\beta,\alpha)$ with an axis-symmetric filter $h(\theta,\phi)$. Starting with the definition of inverse convolution, we get

$$\begin{aligned}
\widehat{x}(\theta,\phi) &= \int_{SO(3)} [D(\alpha,\beta,\gamma)h](\theta,\phi)y(\beta,\alpha)d\rho && (83)\\
&\stackrel{24}{=} \int_{SO(3)} \left[\sum_{l,m}\left(D^l_{m0}(\alpha,\beta,\gamma)h^{l,0}\right)Y^m_l(\theta,\phi)\right] y(\beta,\alpha)d\rho && (84)\\
&\stackrel{29}{=} \int_{SO(3)} \left[\sum_{l,m}\left(D^l_{m0}(\alpha,\beta,\gamma)h^{l,0}\right)\sqrt{\frac{2l+1}{4\pi}}D^{l*}_{m0}(\phi,\theta,\gamma')\right] y(\beta,\alpha)d\rho && (85)\\
&= \int_{SO(3)} \left[\sum_{l,m}\left(D^{l*}_{m0}(\phi,\theta,\gamma')h^{l,0}\right)\sqrt{\frac{2l+1}{4\pi}}D^{l}_{m0}(\alpha,\beta,\gamma)\right] y(\beta,\alpha)d\rho && (86)
\end{aligned}$$

We note that γ and γ' can take on any value without affecting the equation. Continuing, we get

$$\begin{aligned}
\widehat{x}(\theta,\phi) &\stackrel{29}{=} \int_{SO(3)} \left[\sum_{l,m} D^{l*}_{m0}(\phi,\theta,\gamma')h^{l,0}Y^{m*}_l(\beta,\alpha)\right] y(\beta,\alpha)d\rho && (87)\\
&\stackrel{24}{=} \int_{SO(3)} \left[\sum_{l,m} D^{l}_{m0}(\phi,\theta,\gamma')h^{l,0*}Y^{m}_l(\beta,\alpha)\right]^* y(\beta,\alpha)d\rho && (88)\\
&= \int_{SO(3)} \left[D(\phi,\theta,\gamma')h^*\right]^*(\beta,\alpha)y(\beta,\alpha)d\rho && (89)\\
&= \int_0^{2\pi}\int_0^{\pi}\int_0^{2\pi} \left[D(\phi,\theta,\gamma')h^*\right]^*(\beta,\alpha)y(\beta,\alpha)\sin\beta d\alpha d\beta d\gamma && (90)\\
&= 2\pi\int_0^{\pi}\int_0^{2\pi} \left[D(\phi,\theta,\gamma')h^*\right]^*(\beta,\alpha)y(\beta,\alpha)\sin\beta d\alpha d\beta && (91)
\end{aligned}$$

Eq. (91) without the 2π is simply a forward convolution between the spherical image $y(\beta,\alpha)$ (where we remind the readers that α is taking the role of ϕ and β is taking the role of θ) and the filter $h^*(\beta,\alpha)$. Hence using Eq. (17), we get

$$[\widehat{x}(\theta,\phi)]^{l,m} = 2\pi\sqrt{\frac{4\pi}{(2l+1)}}y^{l,m}h^{l,0} \quad (92)$$

ACKNOWLEDGMENT

The authors would like to thank Marshall Tappen for discussion on optimization procedures, Bill Freeman and Ted Adelson for discussion on self-invertibility, and Vivek Goyal for discussion on norm preserving dilations in Euclidean wavelets. Thomas Yeo would like to especially thank Chiao-Lun Cheng for discussion on spherical harmonics and wigner-D functions.

REFERENCES

[1] Antoine, J-P and Vandergheynst, P. Wavelets on the 2-Sphere: a Group-Theoretical Approach. *Applied and Computational Harmonic Analysis*, 7:262–291, 1999.

[2] Bertsekas, D.P. Nonlinear Programming. *Athena Scientific*, 1998.

[3] Bogdanova I., Vandergheynst, P., Antoine, J-P, Jacques, L., and Morvidone, M. Stereographic Wavelet Frames on the Sphere. *Applied and Computational Harmonic Analysis*, 19:223–252, 2005.

[4] Brechbuhler, C.H., Gerig, G., and Kubler O. Parametrization of Closed Surfaces for 3-D Shape Description. *Computer Vision and Image Understanding*, 61(2):154–170, 1994.

[5] Cooley, J.W.; Tukey, J.W. An Algorithm for the Machine Calculation of Complex Fourier Series. *Mathematics of Computation*, 19(90):297–301, 1965.

[6] Daubechies, I. Ten Lectures on Wavelets. *Society for Industrial and Applied Mathematics (SIAM)*, 1992.

[7] Demanet, L. and Vandergheynst, P. Gabor Wavelets on the Sphere. *Wavelets: Applications in Signal and Image Processing, Proceedings of the SPIE*, (5207):208–215, 2003.

[8] Do, M.N., and Vetterli, M. The finite ridgelet transform for image representation. *IEEE Transactions on Image Processing*, 12(1):16–28, 2003.

[9] Driscoll, J.R. and Healy, D.M. Computing Fourier Transforms and Convolutions on the 2-Sphere. *Advances in Applied Mathematics*, 15:202–250, 1994.

[10] Freeden, W. and Windheuser U. Spherical Wavelet Transform and its Discretization *Advances in Computational Mathematics*, 5:51–94, 1996.

[11] Freeden, W., Gervens, T. and Schneider, M. Constructive Approximation on the Sphere: with Applications to Geomathematics. *Clarendon Press, Oxford*, 1998

[12] Freeman, W.T. and Adelson, E.W. The Design and Use of Steerable Filters. *IEEE Transactions Pattern Analysis and Machine Intelligence*, 13(9):891–906, 1991.

[13] Kostelec, P.J. and Rockmore, D.N. A Lite Version of Spharmonic Kit. *http://www.cs.dartmouth.edu/geelong/sphere/*.

[14] Mhaskar, H.N., Narcowich, F.J., Prestin, J., and Ward, J.D. Polynomial frames on the sphere. *Advances in Computational Mathematics*, 13:387-403, 2000.

[15] Papoulis, A. Generalized Sampling Expansion *IEEE Transactions Circuits and Systems*, 24(11):652–654, 1977.

[16] Press, W.H., Teukolsky, S.A., Vetterling, W.T. and Flannery, B.P. Numerical Recipes in C: The Art of Scientific Computing. *Second Edition, Cambridge University Press.*

[17] Sakurai, J.J. Modern Quantum Mechanics *Second Edition, Addison Wesley*, 1994.

[18] Schroder, P. and Sweldens, W. Spherical Wavelets: Efficiently Representing Functions on the Sphere. *Computer Graphics Proceedings (SIGGRAPH)*, 161–172, 1995.

[19] Schroder, P. and Sweldens, W. Spherical Wavelets: Texture Processing. *Rendering Techniques*, 252–263, Aug 1995.

[20] Simoncelli, E.P., Freeman, W.T., Adelson, E.H., and Heeger, D.J. Shiftable Multi-scale Transforms. *IEEE Transaction Information Theory*, 38(2):587–607, 1992.

[21] Starck, J.-L., Candes E.J., and Donoho, D.L. The curvelet transform for image denoising. *IEEE Transactions on Imaging Processing*, 11(6):670–684, 2002.

[22] Starck, J.-L., Abrial, P., Moudden, Y. and Nguyen, M.K. Wavelets, Ridgelets and Curvelets on the sphere. *Astronomy and Astrophysics*, 446:1191–1204, 2006.

[23] Vetterli, M. and Kovačevic, J. Wavelets and Subband Coding. Prentice-Hall, 1995.

[24] Wandelt, B.D. and Gorski, K.M. Fast Convolution on the Sphere. *Physics Review D 63*, 1230002:1–6, 2001.

[25] Wiaux, Y., Jacques, L., and Vandergheynst. P. Correspondence Principle Between Spherical and Euclidean Wavelets. *Astrophysical Journal*, 632:15-28, 2005.

[26] Wiaux, Y., Jacques, L., and Vandergheynst. P. Fast Directional Correlation on the Sphere with Steerable Filters. *Astrophysical Journal*, 652:820-832, 2006.

[27] Yeo, B.T.T., Ou W. and Golland P. Invertible Filter Banks on the 2-Sphere. *Proceedings of ICIP: International Conference in Image Processing*, 2161-2164, 2006.

[28] Yu, P., Grant, P.E., Qi, Y., Han, X., Segonne, F., Pienaar, R., Busa E., Pacheco, J., Makris, N., Buckner, R., Golland, P. and Fischl, B. Cortical Surface Shape Analysis Based on Spherical Wavelets. *IEEE Transaction on Medical Imaging*, 26(4):582–598, 2007.

B.T. Thomas Yeo Biography text here.

Wanmei Ou Biography text here.

Polina Golland Biography text here.